Journal of Nonlinear Modeling and Analysis
Volume 2, Number 2, June 2020, 267–285
http://jnma.ca; http://jnma.ijournal.cn
DOI:10.12150/jnma.2020.267

Spatial Dynamics of a Diffusive Predator-prey Model with Leslie-Gower Functional Response and Strong Allee Effect

Fengru Wei[1], Cuihua Wang[1] and Sanling Yuan[1,†]

Abstract In this paper, spatial dynamics of a diffusive predator-prey model with Leslie-Gower functional response and strong Allee effect is studied. Firstly, we obtain the critical condition of Hopf bifurcation and Turing bifurcation of the PDE model. Secondly, taking self-diffusion coefficient of the prey as bifurcation parameter, the amplitude equations are derived by using multi-scale analysis methods. Finally, numerical simulations are carried out to verify our theoretical results. The simulations show that with the decrease of self-diffusion coefficient of the prey, the preys present three pattern structures: spot pattern, mixed pattern, and stripe pattern. We also observe the transition from spot patterns to stripe patterns of the prey by changing the intrinsic growth rate of the predator. Our results reveal that both diffusion and the intrinsic growth rate play important roles in the spatial distribution of species.

Keywords Predator-prey model, Leslie-Gower functional response, Allee effect, Turing bifurcation, Amplitude equations, Pattern formation.

MSC(2010) 92C15, 39A14.

1. Introduction

Lotka-Volterra equation is the classical model to study the interaction between prey and predator populations, in which the prey population is assumed to be of logistic growth in the absence of predator. It provides the basis for the study of predator-prey model later [1–3]. In actual nature, the resources and environment is constantly changing and the environmental capacity of the predator may has the relation to the number of prey. Leslie-Gower formula can be used to describe exactly this situation, which is introduced by Leslie et al. [4–6], and satisfies the following assumptions [5, 7, 8]:

- The reduction in the number of the predator and individual capture rate is correlated.
- The density of the predator is proportional to the adaptive capacity and the amount of prey.

†the corresponding author.
Email address: Sanling@usst.edu.cn(S. Yuan)
[1]College of Science, University of Shanghai for Science and Technology, Shanghai 200093, China
*The authors are supported by National Natural Science Foundation of China (11671260).

These assumptions emphasize that the growth rate of the predator and prey is not infinite [9], which is in accordance with the situation with the limited resources.

Meanwhile, the prey population is affected by its own density, mate, resources and other factors, which will inhibit or promote the growth of the prey population [10]. Allee effect is one of the most important factors in the study of biological population, which has attracted extensive attention due to its biological significance [11–13]. For instance, Voorn et al. [14] deal with the bifurcation analysis of two predator-prey models with strong Allee effect and it can cause the bistability. Wang et al. [15] studied global bifurcation analysis of a class of general predator-prey models with strong Allee effect in prey population and the results suggest that overexploitation could lead to the extinction of predator-prey populations. In a recent paper [16], Nicole et al. conducted complete qualitative studies of the following model:

$$\begin{cases} \dfrac{du}{dt} = ru(1-\dfrac{u}{K})(1-\dfrac{m+b}{u+b}) - quv, \\ \dfrac{dv}{dt} = sv(1-\dfrac{v}{nu}), \end{cases} \tag{1.1}$$

where $u(t)$ and $v(t)$ are respectively the densities of prey and predator populations; r and s denote respectively the intrinsic growth rates of prey and predator; K represents the environmental capacity of prey; nu represents the environmental carrying capacity of the predator, which characterize Lesile-Gower function response, and $A(u) = 1 - \frac{m+b}{u+b}$ represents the Allee effect [17–19]. Considering the small population extinction rate is higher, it is required that $b > 0$, $-b < m < K$, namely $m + b > 0$. Based on [16], model (1.1) is topologically equivalent to

$$\begin{cases} \dfrac{du}{dt} = ((1-u)(u-M) - Qv(u+B))u^2, \\ \dfrac{dv}{dt} = S(u-v)(u+B)v. \end{cases} \tag{1.2}$$

It is well known that spatial dynamics among predator-prey populations have been one of the main research topics in recent years [20]. Diffusion can also break the stability of equilibrium, which may lead to the generation of spatial pattern. In the primitive spatial ecosystem, the spatial distribution of predator-prey depends on the influence of geographical location, climate, season and other conditions, such as the free movement of species, predator environmental capacity, prey refuge effect and Allee effect. So, in this paper, we consider the effects of diffusion of two species on spatial dynamics of model (1.2). The model has the following form:

$$\begin{cases} \dfrac{\partial u(x,y,t)}{\partial t} = ((1-u)(u-M) - Qv(u+B))u^2 + d_{11}\nabla^2 u, & (x,y) \in \Omega, t > 0, \\ \dfrac{\partial v(x,y,t)}{\partial t} = S(u-v)(u+B)v + d_{22}\nabla^2 v, & (x,y) \in \Omega, t > 0, \\ \dfrac{\partial u}{\partial \mathbf{n}} = \dfrac{\partial v}{\partial \mathbf{n}} = 0, & (x,y) \in \partial\Omega, t > 0 \end{cases} \tag{1.3}$$

with initial conditions:

$$u(x,y,0) \geq 0, \ v(x,y,0) \geq 0,$$

where d_{11} and d_{22} respectively represent the self-diffusion coefficient of prey and predator; the boundary $\partial\Omega$ is smooth and Ω is a bounded region of $\mathbb{R}^N$; the outward

unit normal vector of the boundary $\partial\Omega$ is $\mathbf{n}$. Homogeneous Neumann boundary conditions show that the population on the boundary is zero-flux.

Pattern formation is one of the three main research objects of reaction-diffusion systems [21–25]. As everyone knows, pattern refers to the non-uniform macroscopic structure with some regularity in space or time, there are various temporal-spatial patterns in our living space [26]. For example, the stripe pattern in the animal body surface decorative pattern [27, 28], fluid [29], faraday system of surface wave spot diagram [30], a pattern of chemical reactions [31], bacterial group competition and cooperation of the growth behavior, the space of a linear optical system diagram and gas discharge in the spot diagram [32–34]. In order to master the diversity of spatial distribution of species, it is of great significance to research the pattern dynamics [35–38]. In our work, based on the previous studies of Nicole et al. [16], we mainly discuss the influence of diffusion on the pattern dynamics of model (1.3).

The rest of the paper is organized as follows. In Section 2, Some preliminaries about the existence and stability of the equilibrium of the temporal model is given. Through the method of linear stability analysis, Turing region is shown in Section 3. In section 4, the amplitude equations closed to Turing bifurcation are derived by using standard multi-scale analysis. And some numerical simulations are carried out in Section 5. Finally, we conclude the research and make a summary of our research in Section 6 of this paper.

2. Some preliminaries

Based on the results obtained in [16], we know that model (1.2) always has two boundary equilibria $E_0 = (0, 0)$ and $E_1 = (1, 0)$, and may have another one boundary equilibrium $E_M = (M, 0)$ (if $M > 0$). But from biological point of view, we only pay our attention on the interior equilibrium $\bar{E} = (\bar{u}, \bar{v})$ which satisfies the following equation:

$$(1 - \bar{u})(\bar{u} - M) - Q\bar{u}(\bar{u} + B) = 0, \bar{v} = \bar{u}. \tag{2.1}$$

From Lemma 5 (1) in literature [16], we have

Lemma 2.1. *Assume that* (H_0) $M+1-BQ > 0, (M+1-BQ)^2 - 4(Q+1)M > 0$ *holds, then model* (1.2) *exists two interior equilibria* $E_1 = (u_1, v_1)$ *and* $E_2 = (u_2, v_2)$, *where*

$$u_1 = v_1 = \frac{M + 1 - BQ - \sqrt{(M + 1 - BQ)^2 - 4(Q + 1)M}}{2(Q + 1)},$$

$$u_2 = v_2 = \frac{M + 1 - BQ + \sqrt{(M + 1 - BQ)^2 - 4(Q + 1)M}}{2(Q + 1)}.$$

If (H_0), then the interior equilibrium E_1 of model (1.2) is always a hyperbolic saddle [16], so Turing instability can only occur at interior equilibrium E_2.

The jacobian matrix of model (1.2) at equilibrium $E_2 = (u_2, v_2)$ is

$$J_0 = \begin{pmatrix} a_{11} & a_{12} \\ a_{21} & a_{22} \end{pmatrix} \tag{2.2}$$

where

$$a_{11} = (-4 - 3Q)u_2^3 + (3M + 3 - 2BQ)u_2^2 - 2Mu_2,$$

$$a_{12} = -Qu_2^2(B+u_2),\ a_{21} = Su_2(B+u_2),\ a_{22} = -Su_2(B+u_2).$$

The characteristic equation corresponding to (2.2) can be written as

$$\lambda^2 - Tr_0\lambda + \Delta_0, \tag{2.3}$$

where

$$Tr_0 = -u_2(2M - 3u_2 + 3Qu_2^2 + SB - 3Mu_2 + Su_2 + 4u_2^2 + 2BQu_2),$$

$$\Delta_0 = Su_2^2(B+u_2)(4Pu_2^2 - 3(Q+1)u_2 + 2M).$$

Simple calculation shows that $\Delta_0 < 0$ is always true, and $TrJ_0 < 0$ is equivalent to $S > S_H = \frac{(-4-3Q)u_2^2+(3M+3-2BQ)u_2-2M}{(B+u_2)}$. Suppose that equation (2.3) has a pair of conjugate complex roots of $\beta_1(S) + i\beta_2(S)$, so $\beta_1(S_H) = 0, \beta_2(S_H) = \sqrt{\Delta_0} > 0$ and $\frac{d}{dS}\beta_1(s)\mid_{S=S_H} = -\frac{u_2}{2}(B+u_2) < 0$.

Combine the above analysis, we have the following result.

Theorem 2.1. *Assume that* (H_0) *holds, then the equilibrium* E_2 *of model* (1.2) *is locally asymptotically stable when* $S > S_H$ *and unstable when* $S < S_H$. *A Hopf bifurcation will occur at the equilibrium* E_2 *when* $S = S_H$.

3. Linear stability analysis and the Turing space

In this section, by using of linear stability analysis, we derive the conditions under which the Turing instability of model (1.3) at E_2 occur.

To facilitate the discussion below, we assume the following.

$(H1)$ $a_{11} + a_{22} < 0$;

$(H2)$ $a_{11}d_{22} + a_{22}d_{11} > 0$;

$(H3)$ $a_{11}d_{22} - Su_2(B+u_2)d_{11} - 2\sqrt{d_{11}d_{22}\Delta_0} > 0$.

The Jacobian matrix of model (1.3) at E_2 is

$$J_k = \begin{pmatrix} a_{11} - d_{11}k^2 & a_{12} \\ a_{21} & a_{22} - d_{22}k^2 \end{pmatrix}, \tag{3.1}$$

the determinant and the trace of J_k are respectively

$$\Delta_k = \Delta_0 - [a_{11}d_{22} + a_{22}d_{11}]k^2 + d_{11}d_{22}k^4, \tag{3.2}$$

and

$$Tr_k = Tr_0 - (d_{11} + d_{22})k^2. \tag{3.3}$$

The characteristic equation corresponding to J_k is

$$\lambda^2 - Tr_k\lambda + \Delta_k = 0, \tag{3.4}$$

the roots of Eq.(3.4) are

$$\lambda_{1,2} = \frac{1}{2}Tr_k \pm \frac{1}{2}\sqrt{Tr_k^2 - 4\Delta_k},$$

clearly, $Tr_k < 0$ when (H1) is met, thus, in order to obtain Turing instability we must have $\Delta_k < 0$ for some $k > 0$. If (H_2) holds, then the minimum value of Δ_k is obtained at the critical wave number

$$k_T = \sqrt{\frac{a_{11}d_{22} + a_{22}d_{11}}{2d_{11}d_{22}}}. \tag{3.5}$$

Substitute (3.5) into (3.2), then the condition of Turing instability to occur when

$$(a_{11}d_{22} + a_{22}d_{11})^2 > 4d_{11}d_{22}\Delta_0. \tag{3.6}$$

Considing d_{11} as the branching parameter, then the critical condition for Turing instability to occur is $d = d_{11_T}$, where

$$d_{11_T} = \frac{((4+3Q)u_2^2 - (3M+3-2BQ)u_2 - 2M)d_{22}}{S(B+u_2)}.$$

From the above analysis, we can obtain the following theorem.

Theorem 3.1. *For model* (1.3)*, the Turing instability occurs at* $E_2 = (u_2, v_2)$ *if* $(H0) - (H3)$ *are met.*

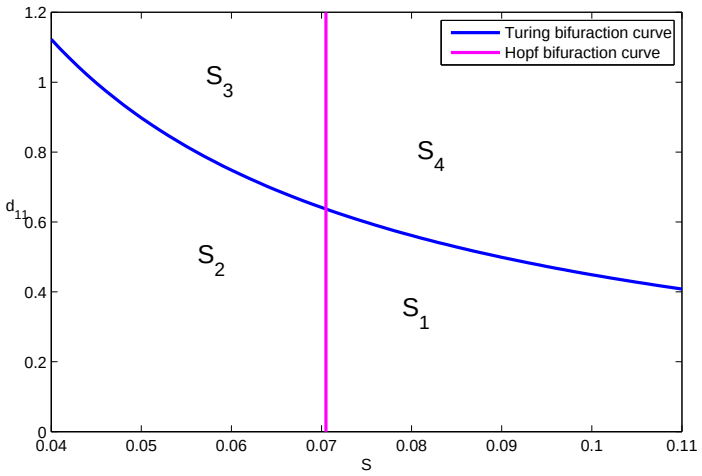

Figure 1. Bifurcation diagram of model (1.3) in $S - d_{11}$ space. With parameters $B = 0.65, M = 0.08, Q = 0.5$, $d_{22} = 5$. The Turing space is denoted by S_1, which is bounded by the blue and the carmine curves. S_2- Turing-Hopf space; S_3- Hopf space; S_4- stable space.

Fig.1 and Fig. 2 are provided for a more intuitive understanding of the Turing space and Turing instability conditions. In Fig.1, fix parameters $B = 0.65, M = 0.08, Q = 0.5, d_{22} = 5$, we show the Turing space in $S - d_{11}$ plane, and the Turing space S_1 is bounded by the blue and the carmine curves. In Fig. 2, we take $S = 0.075$ and other parameter values are the same as in Fig.1. changing the value of d_{11}, we show the correlation between Δ_k and k^2 and the correlation between $Re(\lambda)$ and k^2, the critical parameter value of Turing instability occur is $d_{11_T} = 0.6$. That is to say, the Turing instability occur when $d_{11} < d_{11_T}$.

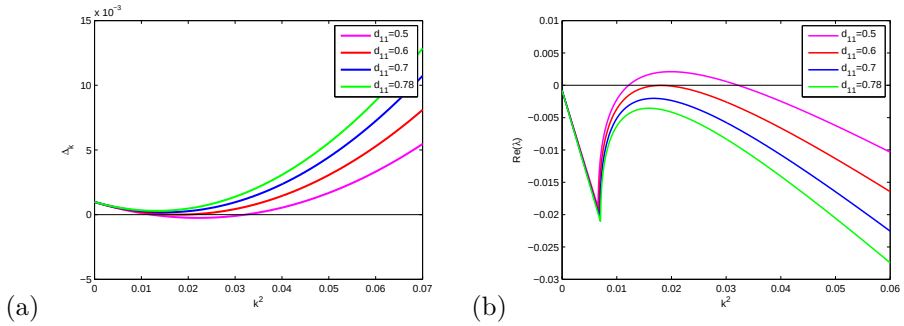

(a) (b)

Figure 2. (a): Plot of Δ_k against k^2 with different d_{11}. (b): Plot of $Re(\lambda)$ against k^2 with different d_{11}. Red line: $d_{11} = d_{11_T} = 0.6$, magenta line: $d_{11} = 0.5$, blue line: $d_{11} = 0.7$, green line: $d_{11} = 0.78$. Other parameter values: $B = 0.65, M = 0.08, Q = 0.5, d_{22} = 5$.

4. The amplitude equations and pattern stability analysis

In this section, we chose d_{11} as the bifurcation parameter and use the standard multi-scale method to derive the amplitude equation of the model (1.3). The detailed derivation process is shown in appendix (A). Below, we give only a brief result of the amplitude equation. We know that the Turing pattern of the model (1.3) is described by the modes composed of three pairs of wave vectors $\boldsymbol{k}_1$, $\boldsymbol{k}_2$ and $\boldsymbol{k}_3$, three pairs of wave vectors form 120° angles to each other. Near the critical point d_{11}=d_{11_T}, setting $U = (u, v)^T$, the solution form of model (1.3) can be written as

$$U = \begin{pmatrix} u \\ v \end{pmatrix} = \sum_{j=1}^{3} \begin{pmatrix} A_j^u \\ A_j^v \end{pmatrix} \exp\left(i\boldsymbol{k}_j \cdot \boldsymbol{r}\right) + c.c., \tag{4.1}$$

where $|\mathbf{k}_j| = k_c$, A_j stands for the oscillation vector of the amplitude, c.c. is the complex conjugate of the right-hand side. The amplitude equations of the entire two-dimensional system Turing spot diagram are

$$\begin{cases} \tau_0 \dfrac{\partial A_1}{\partial t} = \mu A_1 + h\overline{A}_2\overline{A}_3 - \left[g_1|A_1|^2 + g_2\left(|A_2|^2 + |A_3|^2\right)\right] A_1, \\ \tau_0 \dfrac{\partial A_2}{\partial t} = \mu A_2 + h\overline{A}_1\overline{A}_3 - \left[g_1|A_2|^2 + g_2\left(|A_1|^2 + |A_3|^2\right)\right] A_2, \\ \tau_0 \dfrac{\partial A_3}{\partial t} = \mu A_3 + h\overline{A}_1\overline{A}_2 - \left[g_1|A_3|^2 + g_2\left(|A_1|^2 + |A_2|^2\right)\right] A_3. \end{cases} \tag{4.2}$$

Next, we conduct the following linear stability analysis for the amplitude equations, where each amplitude can be described as:

$$A_j = \rho_j e^{j\phi_j}, \ j = 1, 2, 3, \tag{4.3}$$

where ϕ_j is the phase angle. Substituting (4.3) into equation (4.2) gives

$$\tau_0 \frac{\partial \phi}{\partial t} = -h \frac{\rho_1^2\rho_2^2 + \rho_1^2\rho_3^2 + \rho_2^2\rho_3^2}{\rho_1\rho_2\rho_3} \sin\phi,$$

$$\tau_0 \frac{\partial \rho_1}{\partial t} = \mu\rho_1 + h\rho_2\rho_3 \cos\phi - g_1\rho_1^3 - g_2(\rho_2^2 + \rho_3^2)\rho_1,$$

$$\tau_0\frac{\partial\rho_2}{\partial t} = \mu\rho_2 + h\rho_1\rho_3\cos\phi - g_1\rho_2^3 - g_2(\rho_1^2+\rho_3^2)\rho_2,$$
$$\tau_0\frac{\partial\rho_3}{\partial t} = \mu\rho_3 + h\rho_1\rho_2\cos\phi - g_1\rho_3^3 - g_2(\rho_1^2+\rho_2^2)\rho_3,$$

where ϕ=ϕ_1+ϕ_2+ϕ_3. The above equations have four steady-state solutions, their stability conclusions are given in Table 1.

Table 1. Different Turing patterns types of different types of solutions.

Steady state solution	Expression formula	Stability condition	Existence conditions
Homogeneous steady state	$\rho_1=\rho_2=\rho_3=0$	Existence	$\mu<\mu_2$
Stripe patten	$\rho_1=\sqrt{\frac{\mu}{g_1}}\neq 0$ $\rho_2=\rho_3=0$	$\mu>\mu_2$ $\mu_2=0$	$\mu>\mu_3$ $\mu_3=\frac{h^2g_1}{(g_2-g_1)^2}$
Hexagonal pattern	$\rho^+=\frac{\lvert h\rvert+\sqrt{h^2+4(g_1+2g_2)\mu}}{2(g_1+2g_2)}$ $\rho^-=\frac{\lvert h\rvert-\sqrt{h^2+4(g_1+2g_2)\mu}}{2(g_1+2g_2)}$	$\mu>\mu_1$ $\mu_1=\frac{-h^2}{4(g_1+2g_2)}$	$\rho^+:\mu<\mu_4$ $\mu_4=\frac{h^2(2g_1+g_2)}{(g_2-g_1)^2}$
The mixed state	$\rho_1=\frac{\lvert h\rvert}{g_2-g_1}$, $\rho_2=\rho_3=\sqrt{\frac{\mu-g_1\rho_1^2}{g_1+g_2}}$	$\mu>\mu_3$ $g_2>g_1$	unstable

5. Numerical investigation of the pattern formation and selection

In order to verify our theoretical analysis, we choose a two-dimensional space with 200×200 grids. The space step and the time step is set as Δh=1, Δt=0.03 respectively. In our model (1.3), S represents the growth rate of the predator, d_{11} is the self-diffusion coefficient of prey. We will conduct some numerical simulations to view the effect of for these two parameters on pattern formation. During the process of numerical simulations, the predator and the prey always exhibit the same pattern structures, so we only show the spatial distribution of prey population.

5.1. The effect of the varied d_{11} on pattern formation

In this subsection, fixing $B=0.65$, $Q=0.5$, $M=0.08$, $S=0.075$ and changing the self-diffusion coefficient d_{11} located in the Turing space S_1 (Fig.1), we study the effect of the varied d_{11} on pattern formation.

Three basic types of pattern structures are found: cold-spot pattern (Fig.3(f)), mixed pattern (Fig.4(f)) and stipe pattern (Fig.5(f)). When $d_{11}=0.55$, the model (1.3) shows spot pattern (Fig.3). In this case, $\mu=0.0833\in(\mu_2,\mu_3)$. The preys evolve from the stripe with high-density to the structures with cold-spots. With the decrease of d_{11}, when $d_{11}=0.2$, mixed pattern appeared. At this point, $\mu=0.6667\in(\mu_3,\mu_4)$. The cold-spots expand gradually to the cold-stripe and the overall region is occupied by the stripe pattern with few cold-pattern. Finally, if

$d_{11} = 0.05$, the model (1.3) shows the labyrinth pattern. And, we obtain that $\mu = 0.9167 \in (\mu_4, \infty)$. All above results are in accordance with our theoretical analysis.

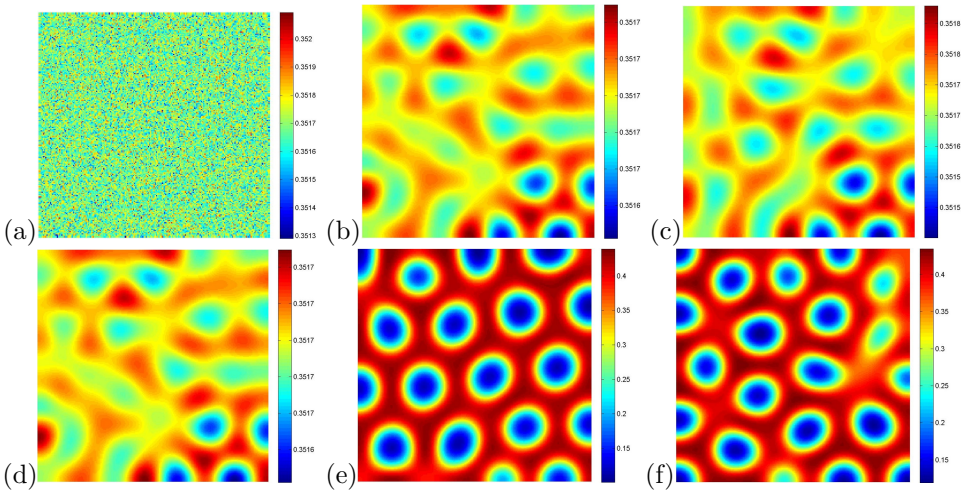

Figure 3. Evolution of prey at different instants with parameters $Q = 0.5, B = 0.65, M = 0.08, S = 0.075, d_{11} = 0.55, d_{22} = 5$. (a) t=0 iterations, (b) t=30000 iterations, (c) t=100000 iterations, (d) t=300000 iterations, (e) t=600000 iterations,(f) t=1000000 iterations.

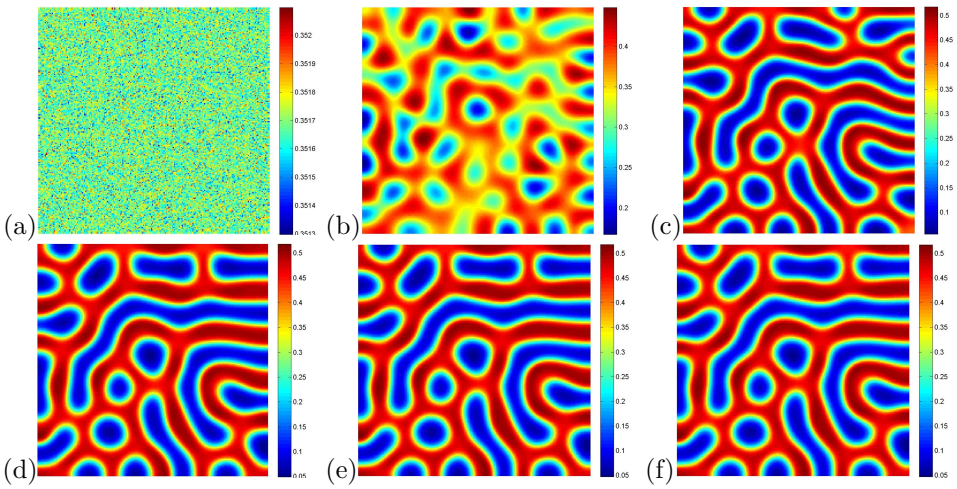

Figure 4. Evolution of prey at different instants with parameters $Q = 0.5, B = 0.65, M = 0.08, S = 0.075, d_{11} = 0.2, d_{22} = 5$. (a) t=0 iterations, (b) t=30000 iterations, (c) t=100000 iterations, (d) t=300000 iterations, (e) t=600000 iterations,(f) t=1000000 iterations.

In order to illustrate the effect of the self-diffusion coefficient d_{11} on the spatial distribution of the preys. We choose six sets of d_{11} and they are $d_{11} = 0.55,\ 0.35,\ 0.2,\ 0.07,\ 0.03,\ 0.01$ respectively. When $d_{11} = 0.55$, the preys show the cold-spot pattern (Fig.6(a)). If we decrease d_{11} until $d_{11} = 0.35$, the cold-spot pattern with few short-stripe occur (Fig.6(b)). As the decrease of d_{11}, we find that the cold-spot pattern decrease gradually and fade away ultimately (Fig.6(b)(c)(d)). Then some stripe pattern emerge and the stripe becomes thin little by little (Fig.6(e)(f)).

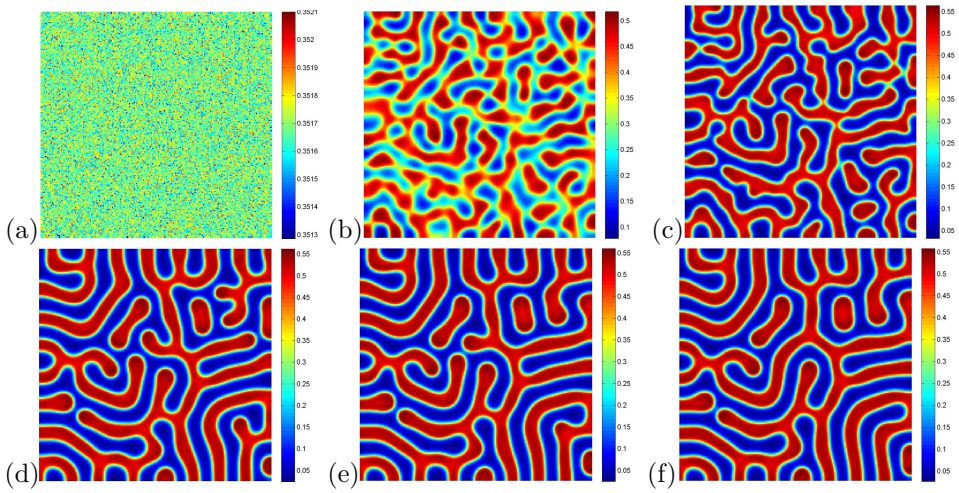

Figure 5. Evolution of prey at different instants with parameters $Q = 0.5, B = 0.65, M = 0.08, S = 0.075, d_{11} = 0.01, d_{22} = 5$. (a) t=0 iterations, (b) t=30000 iterations, (c) t=100000 iterations, (d) t=300000 iterations, (e) t=600000 iterations,(f) t=1000000 iterations.

The pattern transition: cold-spot pattern → mixed pattern → stripe pattern occurs as d_{11} decreases.

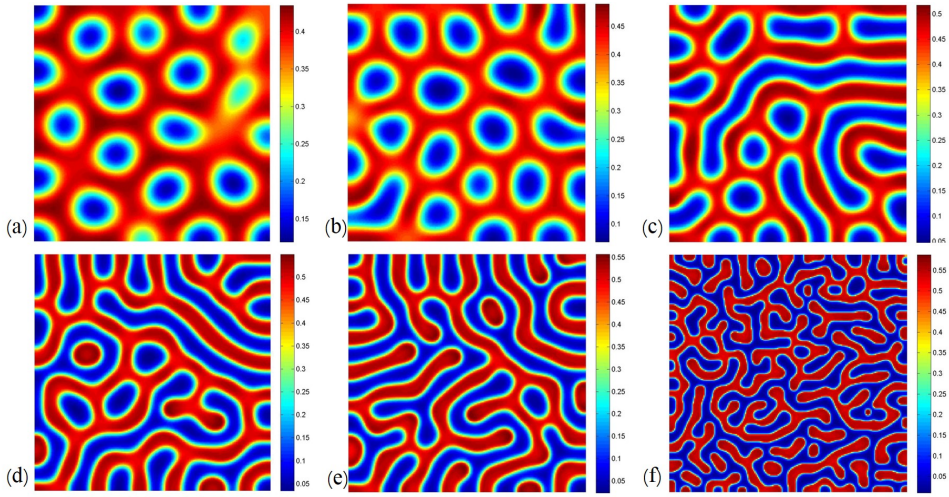

Figure 6. The six categories of Turing pattern of predator at 1000000 iterations with different parameters d_{11}. (a) $d_{11} = 0.55$; (b) $d_{11} = 0.35$; (c) $d_{11} = 0.2$; (d)$d_{11} = 0.1$; (e)$d_{11} = 0.07$; (f)$d_{11} = 0.01$. Other parameters are set as $Q = 0.5, B = 0.65, M = 0.08, S = 0.075, d_{22} = 5$.

5.2. The effect of the varied S on pattern formation

In biology, the intrinsic growth rate S are also an important factor for the density of the population, which may affect the pattern structure. The parameters in Table.

2 are selected for the simulations.

Table 2. Parameters values for simulations.

Q	B	M	S	d_{11}	d_{22}
0.5	0.65	0.08	0.0706	0.05	5
0.5	0.65	0.08	0.4000	0.05	5
0.5	0.65	0.08	0.8500	0.05	5

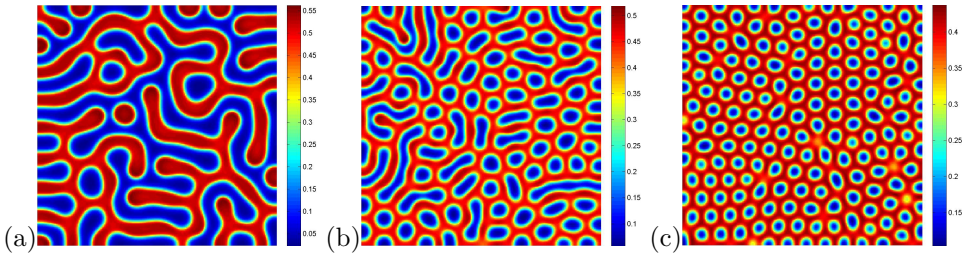

Figure 7. The three categories of Turing pattern of prey at 1000000 iterations with different growth rate S. (a) $S = 0.0706$; (b) $S = 0.4000$; (c) $S = 0.8500$. Other parameters are set as $Q = 0.5, B = 0.65, M = 0.08, S = 0.075, d_{11} = 0.05, d_{22} = 5$.

As can be seen in Fig.7, the increase of the growth rate S also induce the pattern transition: stripe pattern → mixed pattern → cold-spot pattern. When $S = 0.0706$, the model (1.3) shows the stripe pattern with few cold spots (Fig.7(a)). When S increases to 0.4, the stripe becomes thinner and shorter and some tripes break into some spots and thus the overall region is gradually occupied by the mixed pattern with cold-spots and stripes (Fig.7(b)). Finally, if $S = 0.8$, the stripe break completely into cold-spots and these spots decrease gradually (Fig.7(c)).

6. Conclusion and discussion

In this paper, spatial dynamics of a diffusive Leslie-Gower predation model with strong Allee effect is studied. Firstly, according to [16], we obtain the existence conditions of positive equilibrium. Secondly, we derive the critical conditions of Hopf bifurcation and Turing bifurcation in model (1.3). Finally, the appropriate parameters were selected for numerical simulation in the corresponding Turing region. We choose d_{11} as the bifurcation parameter to reveal the influence of self-diffusion on the spatial pattern of the model (1.3). Stripe patterns, mixed patterns and spot patterns are found in our numerical simulations and the pattern transition: cold-spot pattern → mixed pattern → stripe pattern occurs as d_{11} decreases. Meanwhile, the intrinsic growth rate S also can induce the same pattern transition series as S decreases.

Biologically, the diffusion coefficient stands for the remove rate of the preys from the current position and the prey density will decrease as the diffusion coefficient increases, which has the same effect as the decrease of the intrinsic growth rate. In

our model (1.3), the environmental capacity of the predators is positively correlated to the prey density. Thus, if the density of the preys is small, the environmental capacity of the predators is also small. In order to guarantee the coexistence of the preys and the predators, it is necessary to increase the density of the preys. In actual environment, we can add the resources or the opportunity for meeting the mates, which is beneficial to the coexistence of the species. Furthermore, the cross-diffusion, the related parameter of the Allee effect and the Leslie-Gower functional response also have an effect on the pattern dynamics, which need further investigation.

A. Derivation of the amplitude equations

We use the standard multi-scale method to derive the coefficients of amplitude equation of the model (1.3) near the onset d_{11}=d_{11_T}. The solution of model (1.3) can be expressed as

$$\begin{pmatrix} u \\ v \end{pmatrix} = \sum_{j=1}^{3} \begin{pmatrix} A_j^u \\ A_j^v \end{pmatrix} \exp\left(i\boldsymbol{k}_j \cdot \boldsymbol{r}\right) + c.c.. \tag{A.1}$$

The Taylor expansion of model (1.3) at the positive equilibrium point (u_2, v_2) as follows:

$$\begin{cases} \dfrac{\partial u}{\partial t} = d_{11}\nabla^2 u + a_{11}u + a_{12}v + \dfrac{1}{2}f_{20}u^2 \\ \qquad + f_{11}uv + \dfrac{1}{2}f_{02}v^2 + \dfrac{1}{6}f_{30}u^3 + \dfrac{1}{2}f_{21}u^2v + \dfrac{1}{2}f_{12}uv^2 + \dfrac{1}{6}f_{03}v^3 + o(\rho^3), \\ \dfrac{\partial v}{\partial t} = d_{22}\nabla^2 v + a_{21}u + a_{22}v + \dfrac{1}{2}g_{20}u^2 \\ \qquad + g_{11}uv + \dfrac{1}{2}g_{02}v^2 + \dfrac{1}{6}g_{30}u^3 + \dfrac{1}{2}g_{21}u^2v + \dfrac{1}{2}g_{12}uv^2 + \dfrac{1}{6}g_{03}v^3 + o(\rho^3). \end{cases} \tag{A.2}$$

where $a_{11},\ a_{12},\ a_{21},\ a_{22}$ are the same as Eq.(2.1), others are described as follows:

$$\begin{aligned} &f_{20} = (-12 - 6Q)u_2^2 + (6M + 6 - 2BQ)u_2 - 2M, \\ &f_{11} = -3Qu_2^2 - 2BQu_2, \quad f_{02} = 0, \\ &f_{30} = (-24 - 6Q)u_2 + 6(M + 1), \\ &f_{21} = -6Qu_2 - 2BQ, \quad f_{12} = 0, \\ &f_{03} = 0, \\ &g_{20} = 2Su_2, \qquad\qquad g_{11} = BS, \\ &g_{02} = -2S(B + u_2), \qquad g_{30} = 0, \\ &g_{21} = 2S, \quad g_{12} = -2S, \quad g_{03} = 0. \end{aligned}$$

Setting $U = (u, v)^T$, model (1.3) can be transformed into following system:

$$\frac{\partial U}{\partial t} = LU + N, \tag{A.3}$$

where

$$L = L_T + (d_{11} - d_{11_T})M = \begin{pmatrix} a_{11} + d_{11_T}\nabla^2 & a_{12} \\ a_{21} & a_{22} + d_{22}\nabla^2 \end{pmatrix} + (d_{11} - d_{11_T}) \begin{pmatrix} \nabla^2 & 0 \\ 0 & 0 \end{pmatrix},$$

$$N = \begin{pmatrix} \frac{1}{2}f_{20}u^2 + f_{11}uv + \frac{1}{6}f_{30}u^3 + \frac{1}{2}f_{21}u^2v + o(\rho^3) \\ \frac{1}{2}g_{20}u^2 + g_{11}uv + \frac{1}{2}g_{02}v^2 + \frac{1}{2}g_{21}u^2v + \frac{1}{2}g_{12}uv^2 + o(\rho^3) \end{pmatrix}.$$

Then we expand U according to the different order of ε:

$$U = \varepsilon \begin{pmatrix} u_1 \\ u_1 \end{pmatrix} + \varepsilon^2 \begin{pmatrix} u_2 \\ v_2 \end{pmatrix} + \varepsilon^3 \begin{pmatrix} u_3 \\ v_3 \end{pmatrix} + o\left(\varepsilon^3\right). \tag{A.4}$$

At the same time, we expand the controlled variable d_{11} and the nonlinear term N as the following forms:

$$d_{11} - d_{11_T} = \varepsilon d_1 + \varepsilon^2 d_2 + \varepsilon^3 d_3 + o\left(\varepsilon^3\right), \tag{A.5}$$

$$N = \varepsilon^2 N_2 + \varepsilon^3 N_3 + o\left(\varepsilon^3\right), \tag{A.6}$$

where

$$N_2 = \begin{pmatrix} \frac{1}{2}f_{20}{u_1}^2 + f_{11}u_1v_1 \\ \frac{1}{2}g_{20}{u_1}^2 + g_{11}u_1v_1 + g_{02}{v_1}^2 \end{pmatrix}, \tag{A.7}$$

$$N_3 = \begin{pmatrix} f_{20}u_1u_2 + f_{11}(u_1v_2 + u_2v_1) + \frac{1}{2}f_{21}{u_1}^2v_1 + \frac{1}{6}f_{30}{u_1}^3 \\ g_{20}u_1u_2 + g_{11}(u_1v_2 + u_2v_1) + g_{02}v_1v_2 + \frac{1}{2}g_{21}{u_1}^2v_1 + \frac{1}{2}g_{12}u_1{v_1}^2 \end{pmatrix}. \tag{A.8}$$

Next, we derivative the time t to the following term:

$$\frac{\partial}{\partial t} = \varepsilon\frac{\partial}{\partial t_1} + \varepsilon^2\frac{\partial}{\partial t_2} + \varepsilon^3\frac{\partial}{\partial t_3} + o\left(\varepsilon^3\right). \tag{A.9}$$

Substituting Eq.(A.4), (A.5), (A.6), (A.9) into Eq.(A.3), then we can get different order of ε of Eq.(A.3): First order of ε:

$$L_T \begin{pmatrix} u_1 \\ v_1 \end{pmatrix} = 0. \tag{A.10}$$

Second order of ε:

$$L_T \begin{pmatrix} u_2 \\ v_2 \end{pmatrix} = \frac{\partial}{\partial t_1}\begin{pmatrix} u_1 \\ v_1 \end{pmatrix} - d_1 M \begin{pmatrix} u_1 \\ v_1 \end{pmatrix} - N_2. \tag{A.11}$$

Third order of ε:

$$L_T \begin{pmatrix} u_3 \\ v_3 \end{pmatrix} = \frac{\partial}{\partial t_1}\begin{pmatrix} u_2 \\ v_2 \end{pmatrix} + \frac{\partial}{\partial t_2}\begin{pmatrix} u_1 \\ v_1 \end{pmatrix} - d_1 M \begin{pmatrix} u_2 \\ v_2 \end{pmatrix} - d_2 M \begin{pmatrix} u_1 \\ v_1 \end{pmatrix} - N_3. \tag{A.12}$$

For the first order:

$$\begin{pmatrix} u_1 \\ v_1 \end{pmatrix} = \begin{pmatrix} \varphi \\ 1 \end{pmatrix} \left(\sum_{j=1}^{3} W_j \exp\left(i\boldsymbol{k}_j \cdot \boldsymbol{r}\right) \right) + c.c., \tag{A.13}$$

where $\varphi = -\dfrac{a_{22} - d_{22}\widehat{k}_T^2}{a_{21}}$, $\widehat{k}_T^2 = k_T^2|_{d_{11}=d_{11_T}}$, W_j is the amplitude of the corresponding $\exp(i\boldsymbol{k}_j \cdot \boldsymbol{r})$ in the first order.
For the second order:

$$L_T \begin{pmatrix} u_2 \\ v_2 \end{pmatrix} = \frac{\partial}{\partial t_1} \begin{pmatrix} u_1 \\ v_1 \end{pmatrix} - d_1 \begin{pmatrix} \nabla^2 u_1 \\ 0 \end{pmatrix} - \begin{pmatrix} \frac{1}{2} f_{20} {u_1}^2 + f_{11} u_1 v_1 \\ \frac{1}{2} g_{20} {u_1}^2 + g_{11} u_1 v_1 + \frac{1}{2} g_{02} {v_1}^2 \end{pmatrix} \triangleq \begin{pmatrix} F_u \\ F_v \end{pmatrix}. \tag{A.14}$$

Using Fredholm solubility conditions, the vector function at the right side of Eq.(14) must be orthogonal to the zero eigenvector of the adjoint operator ${L_T}^+$ of operator L_T. The zero eigenvector of the operator ${L_T}^+$ is

$$\begin{pmatrix} 1 \\ \psi \end{pmatrix} \exp(-i\boldsymbol{k}_j \cdot \boldsymbol{r}) + c.c., \ j = 1, 2, 3, \tag{A.15}$$

where $\psi = \dfrac{a_{11} - d_{11T}\widehat{k}_T^2}{a_{21}}$. Then base on orthogonal conditions, we obtain:

$$(1, \psi) \begin{pmatrix} F_u^j \\ F_v^j \end{pmatrix} = 0, j = 1, 2, 3, \tag{A.16}$$

where F_u^j, F_v^j denote the coefficients corresponding to $\exp(i\boldsymbol{k}_j \cdot \boldsymbol{r})$ in F_u, F_v respectively. From Eq.(16), we get the following equations:

$$\begin{aligned}
(\varphi + \psi)\frac{\partial W_1}{\partial t_1} &= -d_1 \varphi \widehat{k}_T^2 W_1 + \left(\varphi^2 f_{20} + 2\varphi f_{11} + \psi\left(\varphi^2 g_{20} + 2\varphi g_{11} + g_{02}\right)\right)\overline{W}_2 \overline{W}_3, \\
(\varphi + \psi)\frac{\partial W_2}{\partial t_1} &= -d_1 \varphi \widehat{k}_T^2 W_2 + \left(\varphi^2 f_{20} + 2\varphi f_{11} + \psi\left(\varphi^2 g_{20} + 2\varphi g_{11} + g_{02}\right)\right)\overline{W}_1 \overline{W}_3, \\
(\varphi + \psi)\frac{\partial W_3}{\partial t_1} &= -d_1 \varphi \widehat{k}_T^2 W_3 + \left(\varphi^2 f_{20} + 2\varphi f_{11} + \psi\left(\varphi^2 g_{20} + 2\varphi g_{11} + g_{02}\right)\right)\overline{W}_1 \overline{W}_2.
\end{aligned} \tag{A.17}$$

But it does not give any indication of the asymptotic behavior of the amplitude, thus in order to get more qualitative results, we should push the weak nonlinear analysis to the higher order of the pattern amplitude. Next substituting Eq.(13) into Eq.(14), we can obtain:

$$\begin{aligned}
\begin{pmatrix} u_2 \\ v_2 \end{pmatrix} = &\begin{pmatrix} U_0 \\ V_0 \end{pmatrix} + \sum_{j=1}^{3} \begin{pmatrix} U_j \\ V_j \end{pmatrix} \exp\left(i\boldsymbol{k}_j \cdot \boldsymbol{r}\right) + \sum_{j=1}^{3} \begin{pmatrix} U_{jj} \\ V_{jj} \end{pmatrix} \exp\left(2i\boldsymbol{k}_j \cdot \boldsymbol{r}\right) \\
&+ \begin{pmatrix} U_{12} \\ V_{12} \end{pmatrix} \exp\left(i(\boldsymbol{k}_1 - \boldsymbol{k}_2) \cdot \boldsymbol{r}\right) + \begin{pmatrix} U_{23} \\ V_{23} \end{pmatrix} \exp\left(i(\boldsymbol{k}_2 - \boldsymbol{k}_3) \cdot \boldsymbol{r}\right) \\
&+ \begin{pmatrix} U_{31} \\ V_{31} \end{pmatrix} \exp\left(i(\boldsymbol{k}_3 - \boldsymbol{k}_1) \cdot \boldsymbol{r}\right) + c.c.,
\end{aligned} \tag{A.18}$$

the coefficients in Eq.18 is determined by solving the linear equations of $exp(\boldsymbol{0})$, $exp(i\boldsymbol{k}_j \cdot \boldsymbol{r})$, $exp(i2\boldsymbol{k}_j \cdot \boldsymbol{r})$ and $exp(i(\boldsymbol{k}_j - \boldsymbol{k}_l) \cdot \boldsymbol{r})$, therefore we have

$$\begin{pmatrix} U_0 \\ V_0 \end{pmatrix} = \begin{pmatrix} u^0 \\ v^0 \end{pmatrix} \left(|W_1|^2 + |W_2|^2 + |W_3|^2 \right), U_j = \varphi V_j,$$

$$\begin{pmatrix} U_{jj} \\ V_{jj} \end{pmatrix} = \begin{pmatrix} u^1 \\ v^1 \end{pmatrix} W_j^2, \ \begin{pmatrix} U_{jl} \\ V_{jl} \end{pmatrix} = \begin{pmatrix} u^2 \\ v^2 \end{pmatrix} W_j \overline{W}_l,$$

$$\begin{pmatrix} u^0 \\ v^0 \end{pmatrix} = \begin{pmatrix} \dfrac{2\left(m_1 a_{22} - m_2 a_{12}\right)}{a_{11}a_{22} - a_{12}a_{21}} \\ \dfrac{2\left(m_2 a_{11} - m_1 a_{21}\right)}{a_{11}a_{22} - a_{12}a_{21}} \end{pmatrix},$$

$$\begin{pmatrix} u^1 \\ v^1 \end{pmatrix} = \begin{pmatrix} \dfrac{m_1(a_{22} - 4d_{22}\widehat{k}_T^2) - m_2 a_{12}}{(a_{11} - 4d_{11_T}\widehat{k}_T^2)(a_{22} - 4d_{22}\widehat{k}_T^2) - a_{12}a_{21}} \\ \dfrac{m_2(a_{11} - 4d_{11_T}\widehat{k}_T^2) - m_1 a_{21}}{(a_{11} - 4d_{11_T}\widehat{k}_T^2)(a_{22} - 4d_{22}\widehat{k}_T^2) - a_{12}a_{21}} \end{pmatrix},$$

$$\begin{pmatrix} u^2 \\ v^2 \end{pmatrix} = \begin{pmatrix} \dfrac{2(a_{22} - 3d_{22}\widehat{k}_T^2)m_1 - 2a_{12}m_2}{(a_{11} - 3d_{11_T}\widehat{k}_T^2)(a_{22} - 3d_{22}\widehat{k}_T^2) - a_{12}a_{21}} \\ \dfrac{2(a_{11} - 3d_{11_T}\widehat{k}_T^2)m_2 - 2a_{21}m_1}{(a_{11} - 3d_{11_T}\widehat{k}_T^2)(a_{22} - 3d_{22}\widehat{k}_T^2) - a_{12}a_{21}} \end{pmatrix},$$

in which $m_1 = -(\frac{1}{2}f_{20}\varphi^2 + f_{11}\varphi)$, $m_2 = -(\frac{1}{2}g_{20}\varphi^2 + g_{11}\varphi + \frac{1}{2}g_{02})$.
For the third order: in Eq.12, it is

$$L_T \begin{pmatrix} u_3 \\ v_3 \end{pmatrix} = \frac{\partial}{\partial t_1}\begin{pmatrix} u_2 \\ v_2 \end{pmatrix} + \frac{\partial}{\partial t_2}\begin{pmatrix} u_1 \\ v_1 \end{pmatrix} - d_1 \begin{pmatrix} \nabla^2 u_2 \\ 0 \end{pmatrix} - d_2 \begin{pmatrix} \nabla^2 u_1 \\ 0 \end{pmatrix}$$
$$- \begin{pmatrix} f_{20}u_1u_2 + f_{11}(u_1v_2 + u_2v_1) + \dfrac{1}{2}f_{21}{u_1}^2v_1 + \dfrac{1}{6}f_{30}{u_1}^3 \\ g_{20}u_1u_2 + g_{11}(u_1v_2 + u_2v_1) + g_{02}v_1v_2 + \dfrac{1}{2}g_{21}{u_1}^2v_1 + \dfrac{1}{2}g_{12}u_1{v_1}^2 \end{pmatrix} \triangleq \begin{pmatrix} G_u \\ G_v \end{pmatrix}. \tag{A.19}$$

The coefficient of $exp(i\boldsymbol{k}_j \cdot \boldsymbol{r})$ in Eq.19 is represented by $({G_u}^1, {G_v}^1)^T$, see as follows:

$$
\begin{aligned}
H_u^1 =&\varphi\frac{\partial V_1}{\partial t_1} + \varphi\frac{\partial W_1}{\partial t_2} + d_1\varphi\widehat{k}_T^2 V_1 + d_2\varphi\widehat{k}_T^2 W_1 \\
&- (\varphi f_{20} + f_{11}) \times \left[u^0 W_1 \left(|W_1|^2 + |W_2|^2 + |W_3|^2\right) + \varphi\left(\overline{W}_2\overline{V}_3 + \overline{W}_3\overline{V}_2\right)\right] \\
&- (\varphi f_{20} + f_{11}) \times \left[u^2 W_1 \left(|W_2|^2 + |W_3|^2\right) + u^1 W_1 |W_1|^2\right] \\
&- \varphi f_{11}\left[v^0 W_1 \left(|W_1|^2 + |W_2|^2 + |W_3|^2\right) + \overline{W}_2\overline{V}_3 + \overline{W}_3\overline{V}_2\right] \\
&- \varphi f_{11}\left[v^2 W_1 \left(|W_2|^2 + |W_3|^2\right) + v^1 W_1 |W_1|^2\right] \\
&- \frac{3}{2} f_{21}\varphi^2 W_1 \left(|W_1|^2 + 2|W_2|^2 + 2|W_3|^2\right) \\
&- \frac{1}{2} f_{30}\varphi^3 W_1 \left(|W_1|^2 + 2|W_2|^2 + 2|W_3|^2\right) \\
=&\varphi\frac{\partial V_1}{\partial t_1} + \varphi\frac{\partial W_1}{\partial t_2} + d_1\varphi\widehat{k}_T^2 V_1 + d_2\varphi\widehat{k}_T^2 W_1 \\
&+ \left(I_1|W_1|^2 + I_2\left(|W_2|^2 + |W_3|^2\right)\right) W_1 \\
&- \left(\varphi^2 f_{20} + 2\varphi f_{11}\right)\left(\overline{W}_2\overline{V}_3 + \overline{W}_3\overline{V}_2\right),
\end{aligned}
$$

$$
\begin{aligned}
H_v^1 =&\frac{\partial V_1}{\partial t_1} + \frac{\partial W_1}{\partial t_2} \\
&- (\varphi g_{20} + g_{11}) \times \left[u^0 W_1 \left(|W_1|^2 + |W_2|^2 + |W_3|^2\right) + \varphi\left(\overline{W}_2\overline{V}_3 + \overline{W}_3\overline{V}_2\right)\right] \\
&- (\varphi g_{20} + g_{11}) \times \left[u^2 W_1 \left(|W_2|^2 + |W_3|^2\right) + u^1 W_1 |W_1|^2\right] \\
&- (\varphi g_{11} + g_{02})\left[v^0 W_1 \left(|W_1|^2 + |W_2|^2 + |W_3|^2\right) + \overline{W}_2\overline{V}_3 + \overline{W}_3\overline{V}_2\right] \\
&- (\varphi g_{11} + g_{02})\left[v^2 W_1 \left(|W_2|^2 + |W_3|^2\right) + v^1 W_1 |W_1|^2\right] \\
&- \frac{3}{2}(g_{21}\varphi^2 + g_{12}) W_1 \left(|W_1|^2 + 2|W_2|^2 + 2|W_3|^2\right) \\
=&\frac{\partial V_1}{\partial t_1} + \frac{\partial W_1}{\partial t_2} + \left(J_1|W_1|^2 + J_2\left(|W_2|^2 + |W_3|^2\right)\right) W_1 \\
&- \left(\varphi^2 g_{20} + 2\varphi g_{11} + g_{02}\right)\left(\overline{W}_2\overline{V}_3 + \overline{W}_3\overline{V}_2\right),
\end{aligned}
$$

where

$$
\begin{aligned}
I_1 &= -(\varphi f_{20} + f_{11})(u^0 + u^1) - \varphi f_{11}(v^0 + v^1) - \frac{3}{2}\varphi^2 f_{21} - \frac{1}{2}\varphi^3 f_{30}, \\
I_2 &= -(\varphi f_{20} + f_{11})(u^0 + u^2) - \varphi f_{11}(v^0 + v^2) - 3\varphi^2 f_{21} - \varphi^3 f_{30}, \\
J_1 &= -(\varphi g_{20} + g_{11})(u^0 + u^1) - (\varphi g_{11} + g_{02})(v^0 + v^1) - \frac{3}{2}(\varphi^2 g_{21} + g_{12}), \\
J_2 &= -(\varphi g_{20} + g_{11})(u^0 + u^2) - (\varphi g_{11} + g_{02})(v^0 + v^2) - 3(\varphi^2 g_{21} + g_{12}).
\end{aligned}
$$

Then use Fredholm solubility conditions again, we get that:

$$\begin{cases} \left(\varphi+\psi\right)\left(\dfrac{\partial V_1}{\partial t_1}+\dfrac{\partial W_1}{\partial t_2}\right) = -\widehat{k}_T^2\varphi\left(d_1V_1+d_2W_1\right) \\ \qquad\qquad + \left[\varphi^2 f_{20}+2\varphi f_{11}+\psi\left(\varphi^2 g_{20}+2\varphi g_{11}+g_{02}\right)\right] \\ \qquad\qquad \times\left(\overline{W}_2\overline{V}_3+\overline{W}_3\overline{V}_2\right) \\ \qquad\qquad - [G_1|W_1|^2+G_2(|W_2|^2+|W_3|^2)]W_1, \\ (\varphi+\psi)\left(\dfrac{\partial V_2}{\partial t_1}+\dfrac{\partial W_2}{\partial t_2}\right) = -\widehat{k}_T^2\varphi\left(d_1V_2+d_2W_2\right) \\ \qquad\qquad + \left[\varphi^2 f_{20}+2\varphi f_{11}+\psi\left(\varphi^2 g_{20}+2\varphi g_{11}+g_{02}\right)\right] \\ \qquad\qquad \times\left(\overline{W}_3\overline{V}_1+\overline{W}_1\overline{V}_3\right) \\ \qquad\qquad - [G_1|W_2|^2+G_2(|W_3|^2+|W_1|^2)]W_2, \\ (\varphi+\psi)\left(\dfrac{\partial V_3}{\partial t_1}+\dfrac{\partial W_3}{\partial t_2}\right) = -\widehat{k}_T^2\varphi\left(d_1V_3+d_2W_3\right) \\ \qquad\qquad + \left[\varphi^2 f_{20}+2\varphi f_{11}+\psi\left(\varphi^2 g_{20}+2\varphi g_{11}+g_{02}\right)\right] \\ \qquad\qquad \times\left(\overline{W}_1\overline{V}_2+\overline{W}_2\overline{V}_1\right) \\ \qquad\qquad - [G_1|W_3|^2+G_2(|W_1|^2+|W_2|^2)]W_3, \end{cases} \tag{A.20}$$

in which $G_1=(I_1+\psi J_1), G_2=(I_2+\psi J_2)$. According to Eq.9 the amplitude can be transformed to the following form:

$$\frac{\partial A_j}{\partial t}=\varepsilon\frac{\partial A_j}{\partial t_1}+\varepsilon^2\frac{\partial A_j}{\partial t_2}+\varepsilon^3\frac{\partial A_j}{\partial t_3}+\cdots, \tag{A.21}$$

that is

$$A_j=\varepsilon W_j+\varepsilon^2 V_j+o\left(\varepsilon^3\right).$$

Combining the above derivation and equations, we can get the following amplitude equations corresponding to A_1, A_2, A_3,

$$\begin{cases} \tau_0\dfrac{\partial A_1}{\partial t}=\mu A_1+h\overline{A}_2\overline{A}_3-\left[g_1|A_1|^2+g_2\left(|A_2|^2+|A_3|^2\right)\right]A_1, \\ \tau_0\dfrac{\partial A_2}{\partial t}=\mu A_2+h\overline{A}_1\overline{A}_3-\left[g_1|A_2|^2+g_2\left(|A_1|^2+|A_3|^2\right)\right]A_2, \\ \tau_0\dfrac{\partial A_3}{\partial t}=\mu A_3+h\overline{A}_1\overline{A}_2-\left[g_1|A_3|^2+g_2\left(|A_1|^2+|A_2|^2\right)\right]A_3, \end{cases} \tag{A.22}$$

where

$$\tau_0=-\frac{\varphi+\psi}{d_{11_T}\varphi\widehat{k}_T^2},\quad \mu=\frac{d_{11_T}-d_{11}}{d_{11_T}},\quad h=-\frac{-2m_1-2\psi m_2}{d_{11_T}\varphi\widehat{k}_T^2},$$

$$g_1=-\frac{G_1}{d_{11_T}\varphi\widehat{k}_T^2},\quad g_2=-\frac{G_2}{d_{11_T}\varphi\widehat{k}_T^2}.$$

Next, we conduct the following linear stability analysis for the amplitude equation, where each amplitude can be described as:

$$A_j{=}\rho_j e^{j\phi_j}, \tag{A.23}$$

where ϕ_j is the phase angle corresponding to mode ρ_j, $j = 1, 2, 3$. We substitute Eq.(A.23) into Eq.(A.22), and yield four equations of the real variables as follows:

$$\tau_0 \frac{\partial \phi}{\partial t} = -h \frac{\rho_1^2\rho_2^2 + \rho_1^2\rho_3^2 + \rho_2^2\rho_3^2}{\rho_1\rho_2\rho_3} \sin\phi,$$

$$\tau_0 \frac{\partial \rho_1}{\partial t} = \mu\rho_1 + h\rho_2\rho_3 \cos\phi - g_1\rho_1^3 - g_2(\rho_2^2 + \rho_3^2)\rho_1,$$

$$\tau_0 \frac{\partial \rho_2}{\partial t} = \mu\rho_2 + h\rho_1\rho_3 \cos\phi - g_1\rho_2^3 - g_2(\rho_1^2 + \rho_3^2)\rho_2,$$

$$\tau_0 \frac{\partial \rho_3}{\partial t} = \mu\rho_3 + h\rho_1\rho_2 \cos\phi - g_1\rho_3^3 - g_2(\rho_1^2 + \rho_2^2)\rho_3,$$

where ϕ=ϕ_1+ϕ_2+ϕ_3. Clearly $\mu > 0$. To make ensure that there is the steady state solution above equation, system g_1, g_2 must be positive.

Acknowledgements

This work was supported by the National Natural Science Foundation of China (No.11671260).

References

[1] Y. L. Song, T. Yin and H. Y. Shu, *Dynamics of a ratio-dependent stage-structured predator-prey model with delay*, Mathematical Methods in the Applied Sciences, 2017, 40(18).

[2] G. H. Zhang, W. D. Wang and X. L. Wang, *Coexistence states for a diffusive one-prey and two-predators model with B-D functional response*, Journal of Mathematical Analysis and Applications, 2017, 387(2), 931-948.

[3] G. Q. Sun, C. H. Wang and L. L. Chang et al., *Effects of feedback regulation on vegetation patterns in semi-arid environments*, Applied Mathematical Modelling, 2018, 61, 200-215.

[4] P. H. Leslie, *Some furher notes on the use of matrices in population mathematcis*, Biometrika, 1948, 35(3/4), 213-245.

[5] P. H. Leslie and J. C. Gower, *The properties of a stochastic model for the predator-prey type of interaction between two species*, Biometrika, 1960, 47(3/4), 219-234.

[6] R. Levins, *An introduction to mathematical ecology*, Ecology, 1970, 24(2), 482-482..

[7] Y. Kuang, *Uniqueness of limit cycles in Gause-Type models of predator-prey systems*, Mathematical Biosciences, 1988, 88(1), 67-84.

[8] Y. Kuang, *Rich dynamics of Gause-Type ratio-dependent predator-prey system*, Fields Institute Communications, 1999, 21, 325-337.

[9] S. Gakkhar and B. Singh, *Dynamics of modified Leslie-Gower-type prey-predator model with seasonally varying parameters*, Chaos, Solitons and Fractals, 2006, 27(5), 1239-1255.

[10] X. Y. Meng, N. N. Qin and H. F. Huo, *Dynamics analysis of a predator-prey system with harvesting prey and disease in prey species*, Journal of Biological Dynamics, 2018, 12(1), 342-374.

[11] C. M. Taylor and A. Hastings, *Allee effects in biological invasions*, Ecology Letters, 2005, 8(8), 895-908.

[12] W. C. Allee, *Animal aggregations: a study in general sociology*, University of Chicago Press, 1931.

[13] D.Y. Wu and H. Y. Zhao, *Complex dynamics of a discrete predator-prey model with the prey subject to the Allee effect*, Journal of Difference Equations and Applications, 2017, 1-42.

[14] Voorn, A. George and K. Van et al., *Heteroclinic orbits indicate overexploitation in predator-prey systems with a strong Allee effect*, Mathematical Biosciences, 2007, 209(2), 451-469.

[15] J. Wang, J. Shi and J. Wei, *Predator-prey system with strong Allee effect in prey*, Journal of Mathematical Biology, 2011, 62(3), 291-331.

[16] N. M. Jeraldo and P. Aguirre, *Allee effect acting on the prey species in a Leslie-Gower predation model*, Nonlinear Analysis: Real World Applications, 2019, 45, 895-917.

[17] F. Courchamp, T. H. Clutton-Brock and B. T. Grenfell, *Multipack dynamics and the Allee effect in the African wild dog, Lycaon pictus*, Animal Conservation, 2000, 3(04), 277-285.

[18] F. Courchamp, B. T. Grenfell and T. H. Clutton-Brock, *Impact of natural enemies on obligately cooperative breeders*, Oikos, 2000, 91(2), 311-322.

[19] D. Boukal and L. Berec, *Single-species models of the Allee effect: extinction boundaries, sex ratios and mate encounters*, Journal of Theoretical Biology, 2002, 218(3), 375-394.

[20] C. Ji, D. Jiang and N. Shi, *Analysis of a predator-prey model with modified Leslie-Gower and Holling-type II schemes with stochastic perturbation*, Journal of Mathematical Analysis and Applications, 2009, 359(2), 482-498.

[21] Y. Wang, J. Cao and G. Q. Sun et al., *Effect of time delay on pattern dynamics in a spatial epidemic model*, Physica A: Statistical Mechanics and its Applications, 2014, 412, 137-148.

[22] R. S. Cantrell and C. Cosner, *Spatial ecology via reaction-diffusion equations*, John Wiley and Sons, 2004.

[23] Y. Song, H. Jiang and Y. Yuan, *Turing-Hopf bifurcation in the reaction-diffusion system with delay and application to a diffusive predator-prey model*, Journal of Applied Analysis and Computation, 2019, 9(3), 1132-1164.

[24] D. Jia, T. Zhang and S. Yuan, *Pattern Dynamics of a Diffusive Toxin Producing Phytoplankton-Zooplankton Model with Three-Dimensional Patch*, International Journal of Bifurcation and Chaos, 2019, 29(04), 1930011.

[25] Y. Song, S. Wu and H. Wang, *Spatiotemporal dynamics in the single population model with memory-based diffusion and nonlocal effect*, Journal of Differential Equations, 2019, 267, 6316-6351.

[26] P. Legendre and M. J. Fortin, *Spatial pattern and ecological analysis*, Vegetatio, 1989, 80(2), 107-138.

[27] S. Kondo, *The reaction-diffusion system: a mechanism for autonomous pattern formation in the animal skin*, Genes to Cells, 2002, 7(6), 535-541.

[28] S. Kondo, *How animals get their skin patterns: fish pigment pattern as a live Turing wave*, The International Journal of Developmental Biology, 2009, 53(5-6), 851-856.

[29] G. A. Houseman, M. K. Dan and P. Molnar, *Convective instability of a thickened boundary layer and its relevance for the thermal evolution of continental convergent belts*, Journal of Geophysical Research: Solid Earth, 1981, 86(B7), 6115-6132.

[30] L. Jiang, C. L. Ting and M. Perlin et al., *Moderate and steep faraday waves: instabilities, modulation and temporal asymmetries*, Journal of Fluid Mechanics, 1996, 329, 275-307.

[31] J. Jin, J. Shi and J. Wei et al., *Bifurcations of patterned solutions in the diffusive Lengyel-Epstein system of cima chemical reactions*, The Rocky Mountain Journal of Mathematics, 2013, 1637-1674.

[32] I. Golding, Y. Kozlovsky and I. Cohen et al., *Studies of bacterial branching growth using reaction-diffusion models for colonial development*, Physica A: Statistical Mechanics and its Applications, 1998, 260(3-4), 510-554.

[33] J. E. Gates and D. R. Evans, *Cowbirds breeding in the central appalachians: spatial and temporal patterns and habitat selection*, Ecological Applications, 1998, 8(1), 27-40.

[34] T. Sugawara and K. Kaneko, *Pattern dynamics in a two-dimensional gas discharge system*, Progress of Theoretical Physics Supplement, 2006, 161, 344-347.

[35] Southwood and R. E. Thomas, *Habitat, the templet for ecological Strategies*?, Journal of animal ecology, 1977, 46(2), 336-365.

[36] J. Yang, T. Zhang and S. Yuan, *Turing pattern induced by cross-diffusion in a predator-prey model with pack predation-herd behavior*, International Journal of Bifurcation and Chaos, 2019, doi: S021812742050100X.

[37] Q. Li, Z. Liu and S. Yuan, *Cross-diffusion induced Turing instability for a competition model with saturation effect*, Applied Mathematics and Computation, 2019, 347, 64-77.

[38] S. Yuan, C. Xu and T. Zhang, *Spatial dynamics in a predator-prey model with herd behavior*, Chaos An Interdisciplinary Journal of Nonlinear Science, 2013, 23(3), 033102.